



1 Characteristics of ambient seismic noise as a source for 2 surface wave tomography

3 **Yingjie Yang and Michael H. Ritzwoller**

4 *Center for Imaging the Earth's Interior, Department of Physics, University of Colorado, Boulder, Colorado 80309-0390,*
5 *USA (yingjie.yang@colorado.edu)*

6 [1] Interstation cross correlations of ambient seismic noise from 1 year of continuous data at periods
7 between 6 and 50 s are used to study the origin of the ambient noise using stations located in Europe,
8 southern Africa, Asia, and three regions within North America. The signal-to-noise ratios (SNR) of
9 Rayleigh waves for positive and negative correlation time lags at periods of 8, 14, 25 and 50 s are used to
10 determine the azimuthal distribution of strong ambient noise sources. Ambient noise in both the primary
11 (10–20 s) and secondary microseism bands (5–10 s) comes dominantly from the directions of relatively
12 nearby coastlines with stronger noise occurring in the Northern Hemisphere in northern winter and in the
13 Southern Hemisphere in southern winter, consistent with the hypothesis that oceanic microseisms are
14 generating this noise. The observed differences in the directivity of noise in the primary and secondary
15 microseism bands are the consequence of propagation and attenuation, rather than the location of
16 generation. At intermediate and long periods (>20 s), there is much less seasonal variation in both signal
17 strength and directivity. We argue that our results are explained most simply by near-coastal sources rather
18 than deep ocean sources at all periods. Although the dominant ambient noise sources are distributed
19 inhomogeneously in azimuth, strong ambient noise emerges from most directions when using recordings
20 that are 1 year in duration. Simulations illustrate that this is what ensures the accuracy of the empirical
21 Green's functions and ambient noise tomography.

22 **Components:** 8563 words, 14 figures.

23 **Keywords:** ambient seismic noise; cross correlations; Green's functions; tomography.

24 **Index Terms:** 7255 Seismology: Surface waves and free oscillations; 7270 Seismology: Tomography (6982, 8180).

25 **Received** 4 September 2007; **Revised** 17 November 2007; **Accepted** 30 November 2007; **Published** XX Month 2008.

26 Yang, Y., and M. H. Ritzwoller (2008), Characteristics of ambient seismic noise as a source for surface wave tomography,
27 *Geochem. Geophys. Geosyst.*, 9, XXXXXX, doi:10.1029/2007GC001814.

29 1. Introduction

30 [2] Theoretical and experimental research has
31 shown that the cross correlation of ambient noise
32 records from two receivers provides an estimate of
33 the empirical Green's function between the
34 receivers [Weaver and Lobkis, 2001, 2004; Derode
35 *et al.*, 2003a; Snieder, 2004; Larose *et al.*, 2005].

In seismology, two types of signals have been 36
considered to form random wavefields. The first 37
is seismic coda, which results from the multiple 38
scattering of seismic waves by small-scale inho- 39
mogeneities [e.g., Aki and Chouet, 1975; Paul *et* 40
al., 2005]. The second is ambient seismic noise. 41
Ambient noise, in contrast with seismic coda, has 42
the advantage that it does not depend on earth- 43



44 quake occurrence and can be recorded at any time
45 and any location.

46 [3] Recently, surface wave tomography for Rayleigh
47 waves based on the empirical Green's functions
48 obtained from cross correlations of ambient seismic
49 noise has been applied successfully to real data at
50 regional scales, such as in the western United States
51 [Shapiro *et al.*, 2005; Sabra *et al.*, 2005; Moschetti
52 *et al.*, 2007; Lin *et al.*, 2008], South Korea [Cho
53 *et al.*, 2007], Tibet [Yao *et al.*, 2006], New Zealand
54 [Lin *et al.*, 2007], Iceland [Gudmundsson *et al.*,
55 2007], and southern Africa (Y. Yang *et al.*, Crustal
56 and uppermost mantle structure in southern
57 Africa revealed from ambient noise and teleseis-
58 mic tomography, submitted to *Geophysical Journal*
59 *International*, 2007, hereinafter referred to as Yang
60 *et al.*, submitted manuscript, 2007), and at conti-
61 nental scales, such as in Europe [Yang *et al.*, 2007]
62 and North America [Bensen *et al.*, 2007b]. The
63 basic assumption underlying ambient noise tomog-
64 raphy is that ambient seismic noise can be consid-
65 ered to be composed of randomly distributed
66 wavefields when taken over sufficiently long times,
67 such as a year. A perfectly random distribution of
68 the sources of ambient noise would result in
69 symmetric cross correlations with energy arriving
70 at both positive and negative correlation lag times,
71 usually referred to as the causal and acausal arriv-
72 als. In practice, however, significant asymmetry of
73 the cross correlations is often observed, which
74 results from stronger or closer ambient noise sour-
75 ces directed radially away from one station than the
76 other. Although Derode *et al.* [2003b] showed
77 experimentally that inhomogeneous source distri-
78 butions have lesser effects on the travel times of the
79 waves than on their signal-to-noise ratios, such
80 source distributions may interfere at some level
81 with the ability to obtain reliable Green's functions
82 and measure dispersion curves on them. A better
83 understanding of the origin of ambient noise sour-
84 ces and their temporal and spatial distribution is
85 needed, therefore, to ensure that ambient noise
86 tomography is being developed on a firm footing.

87 [4] Ambient seismic noise in the short-period [4]
88 (<20 s), commonly referred to as microseisms, is
89 considered to be related to the interaction of ocean
90 swells with the seafloor near coastlines. Two strong
91 peaks of the short-period seismic noise are typically
92 observed in the primary (10–20 s) and secondary
93 (5–10 s) microseism bands. The exact generation
94 mechanism of the microseisms is not completely
95 understood, but it is commonly believed that the
96 primary microseism involves direct interaction of

ocean swells with the shallow seafloor [Hasselmann, 97
1963], and the secondary microseism, with double- 98
frequency signals relative to the primary micro- 99
seism, is generated by the nonlinear interaction 100
between the two same frequency primary waves 101
but propagating in opposite directions [Longuet- 102
Higgins, 1950]. Such nonlinear interaction of two 103
oppositely propagating waves may arise near the 104
center of cyclonic depression at the deep sea or 105
near the costal regions where the direct waves and 106
coastline-reflected waves interfere. Long-period 107
seismic noise, referred to as earth “hum,” is 108
observed in the continuous background free oscil- 109
lations in low-frequency seismic spectra [Nawa *et* 110
al., 1998]. This term is usually reserved for 111
motions with periods above 100 s. Early studies 112
attributed the long-period noise to atmospheric 113
motions [Tanimoto and Um, 1999; Ekstrom, 114
2001], but more recent studies [Tanimoto, 2005; 115
Rhie and Romanowicz, 2004, 2006] suggest that 116
the origin of the long-period noise is more likely 117
related to so-called ocean infragravity waves, a long- 118
period ocean gravity wave. Rhie and Romanowicz 119
[2004] proposed that the generation of long-period 120
seismic noise involves a three stage atmosphere- 121
ocean-seafloor coupling process. 122

[5] The procedure to use long-duration cross cor- 123
relations to study the long-range correlation prop- 124
erties of ambient seismic noise was developed by 125
Stehly *et al.* [2006]. They applied the method to 126
about 20 stations in each of California, the eastern 127
United States, Europe, and Tanzania and found that 128
ambient noise in the secondary microseism band is 129
seasonally stable and emerges predominantly from 130
nearby coastlines. In contrast, the primary micro- 131
seism and longer-period ambient noise (below 40 s 132
period) vary seasonally in similar ways and emerge 133
from directions that may not be toward the local 134
coasts. This observation appeared to them to sever 135
the hypothesized physical link between the primary 136
and secondary microseisms, and called into ques- 137
tion the commonly believed casual relation be- 138
tween these waves. These authors argue that the 139
cause of the primary microseism and the longer- 140
period ambient noise is ocean wave activity in deep 141
water. This conclusion is at variance with the study 142
of Rhie and Romanowicz [2006], which is based on 143
detailed observations performed on seismic arrays 144
in Japan and California during a large storm in the 145
Pacific. Rhie and Romanowicz conclude that at all 146
periods, from the secondary microseism at several 147
seconds period to earth hum at 240 s, ocean wave 148
energy is coupled to the solid earth predominantly 149
near coastlines. They argue that nonlinear ocean 150

151 wave-wave interactions near the coast generate
 152 long-period energy, which propagates globally
 153 both as seismic waves in the solid earth and
 154 infragravity waves in the ocean which can then
 155 liberate their energy to the solid earth later, else-
 156 where. This mechanism may imply that ambient
 157 noise is not uniformly distributed in time or space,
 158 which may vitiate assumptions that underlie ambi-
 159 ent noise tomography, however.

160 [6] In this study, we follow the methodology of
 161 *Stehly et al.* [2006], but apply the method to a
 162 much larger station set in Europe, southern Africa,
 163 Tibet, and North America using 12 months of
 164 ambient noise data over a broad period band from
 165 6 to 50 s, which covers the microseism band as
 166 well as longer-period noise. By analyzing the
 167 strength and quality of the cross correlations in
 168 different seasons, directions, and period bands, we
 169 address three principal questions. First, we consider
 170 whether the primary and secondary microseisms
 171 behave differently on average and, hence, may be
 172 physically decoupled. Second, we ask whether the
 173 observations are consistent with generation in shal-
 174 low coastal waters at all periods or require a
 175 deepwater source at long periods. Finally, we
 176 consider whether the resulting azimuthal distribu-
 177 tion of ambient seismic noise is sufficiently homo-
 178 geneous when taken over long times for ambient
 179 noise tomography to be successful. We focus on
 180 Rayleigh waves, so the results for Love waves may
 181 differ. We proceed by first looking at results from
 182 Europe, and then bring in results using arrays in
 183 southern Africa, Tibet, and North America.

184 [7] Throughout the paper, we will refer to the
 185 “source” of ambient noise, and our use of this
 186 term requires clarification. By “source location,”
 187 we refer to the place or places where seismic waves
 188 within the solid earth are generated. The proximate
 189 cause of the seismic waves may be the interaction
 190 of gravity waves in the ocean with the seafloor.
 191 Identification of the ultimate cause of ambient
 192 noise involves a regress of physical mechanisms
 193 that may have involved the generation of ocean
 194 gravity waves, the generation of large ocean storms
 195 from the interaction of winds with the ocean
 196 surface, storm formation in the atmosphere, differ-
 197 ential solar forcing, and so on. Seismic waves,
 198 however, are blind to all processes that occurred
 199 prior to their generation, although the location of
 200 their formation, their frequency content, seasonal
 201 variability, and radiation pattern may provide clues
 202 about earlier processes. Thus, by the “source,”
 203 “source location,” “generation” and “cause,” we

will refer only to that place where and mechanism 204
 by which the seismic waves are generated. 205

[8] Finally, it is important to acknowledge at the 206
 outset that the method of source characterization 207
 that we use is ambiguous and the arguments 208
 presented herein are qualitative in nature. The 209
 method is only capable of determining the relative 210
 direction to the principal source locations observed 211
 at an array, and inferences drawn about absolute 212
 locations must be made on the basis of plausibility 213
 and simplicity. We attempt to make that clear when 214
 simplicity based on the principle is assumed. 215

2. Initial Analysis: Cross Correlations 216 of Ambient Noise in Europe 217

[9] We use continuous vertical component seismic 218
 data from ~125 stations from the Global Seismic 219
 Network (GSN) and the Virtual European Broad- 220
 band Seismic Network (VEBSN) (Figure 1) over 221
 the 12 months of 2004. The data processing 222
 procedure applied here is similar to that described 223
 at length by *Bensen et al.* [2007a]. Raw seismic 224
 data are processed one day at a time for each 225
 station after being decimated to 1 sample per 226
 second, and are band-pass filtered in the period 227
 band from 5 to 50 s after the daily trend, the mean 228
 and the instrument response are removed. Filtered 229
 daily data are then normalized in time and whit- 230
 ened in this frequency band to remove earthquake 231
 signals and instrumental irregularities prior to 232
 performing cross correlation. Daily cross correla- 233
 tions are computed between all station pairs and are 234
 then added to one another or stacked to produce 235
 two 5-month and one 1-year time series. The two 236
 5-month stacks are centered on January and July 237
 respectively; namely, months 11, 12, 1, 2, 3 and 238
 months 5, 6, 7, 8, 9. The 5-month stacks are used to 239
 investigate the seasonal variability of the ambient 240
 noise source. 241

[10] Examples of 12-month cross correlations are 242
 plotted in Figure 2 with the corresponding path 243
 segments shown in the bottom map. For each cross 244
 correlation, surface wave signals coming from the 245
 two opposite directions between the stations appear 246
 at positive (casual component) and negative 247
 (acausal component) correlation time lag, respec- 248
 tively. The incoming directions of seismic noise 249
 contributing to the positive components are marked 250
 with arrows showing the directions of propagation 251
 along each path segment in Figure 2f. The positive 252
 components are for waves coming mostly from the 253
 northerly direction. The amplitude of the causal 254

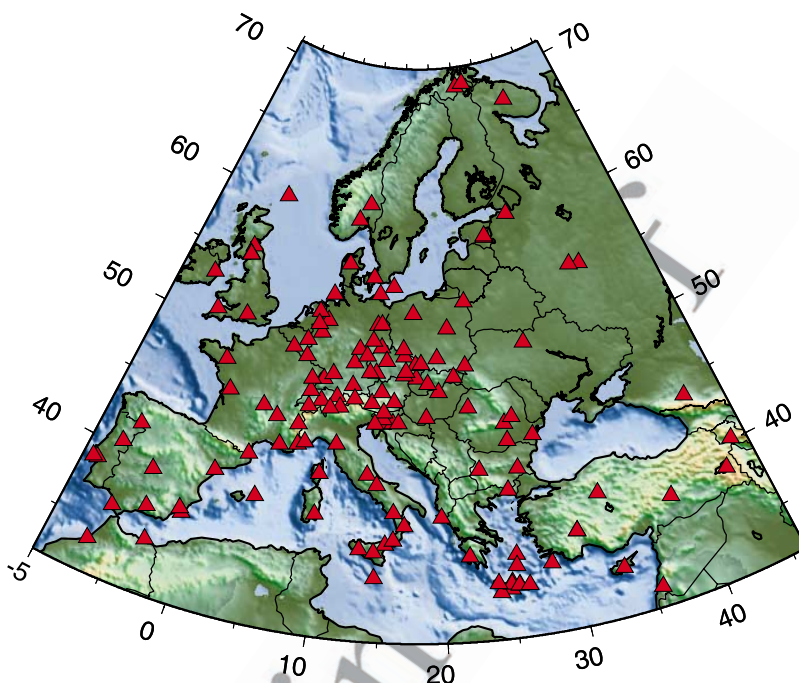


Figure 1. Broadband seismic stations in Europe used in this study, marked by red triangles.

255 and acausal components depends on the strength
256 and density of sources of ambient noise in line with
257 the stations. Although signals coming from oppo-
258 site directions sample the same structure between a
259 station pair, the source characteristics, such as
260 distance, strength, duration, frequency content
261 and so on, may be very different on the two
262 opposite sides. Thus the resulting cross correlations
263 are often asymmetric, as illustrated in Figure 2, and
264 these properties may be period-dependent. For
265 example, the higher-amplitude arrivals in Figure 2
266 are generally from the north, i.e., at positive lag.
267 The negative lag components for station pairs
268 ECH-TUE and DSB-TUE are nearly flat, indicat-
269 ing that there is relatively little energy arriving
270 from the southeast. There is, however, substantial
271 energy at negative lags for the pairs GRFO-TUE,
272 MORC-TUE and KWP-TUE, resulting from waves
273 coming from the southwest. There is also appar-
274 ently a difference in frequency content at positive
275 and negative lags. The best example is probably
276 MORC-TUE, where a clear low-frequency precur-
277 sor appears at positive lag (coming from the
278 northeast), which is missing at negative lag.

279 [11] To demonstrate the frequency content of the
280 signals in Figure 2, we plot in Figure 3 normalized
281 amplitude spectra of the positive (Figures 3f–3j)

and negative (Figures 3a–3e) lag components of
the corresponding cross-correlation time series. In
each case, 1000-s time series are used to compute
the spectrum, starting from zero lag. The lower
curve in each panel is the normalized spectrum of
trailing noise contained in the 1000 s time window
starting at ± 1000 s lag time, which is always well
removed from the surface wave signals. To illus-
trate the frequency-dependent characteristics of
ambient noise sources, we divide the entire fre-
quency band into three subbands: namely, low-
frequency noise LFN (0–0.05 Hz), the primary
microseism band MS1 (0.05–0.1 Hz), and the
secondary microseism band MS2 (0.1–0.2 Hz).
For cross correlations between the station pairs
GRFO-TUE, MORC-TUE and KWP-TUE, there
are strong low-frequency noise signals on the
positive components (Figures 2b–2d and 3g–3i),
which come from the northeast quadrant (Figure 2f).
For the cross correlations ECH-TUE and DSB-
TUE, strong microseismic noise signals are
observed on the positive components (Figures 2a,
2e, 3f, and 3j), coming from the northwest quadrant,
but little energy is observed in the low-frequency
band. The lack of high-frequency noise from a
particular direction probably is a consequence of a
distant source region. The frequency-dependent
characteristics of noise signals in strength and
incoming direction are discussed in more detail in

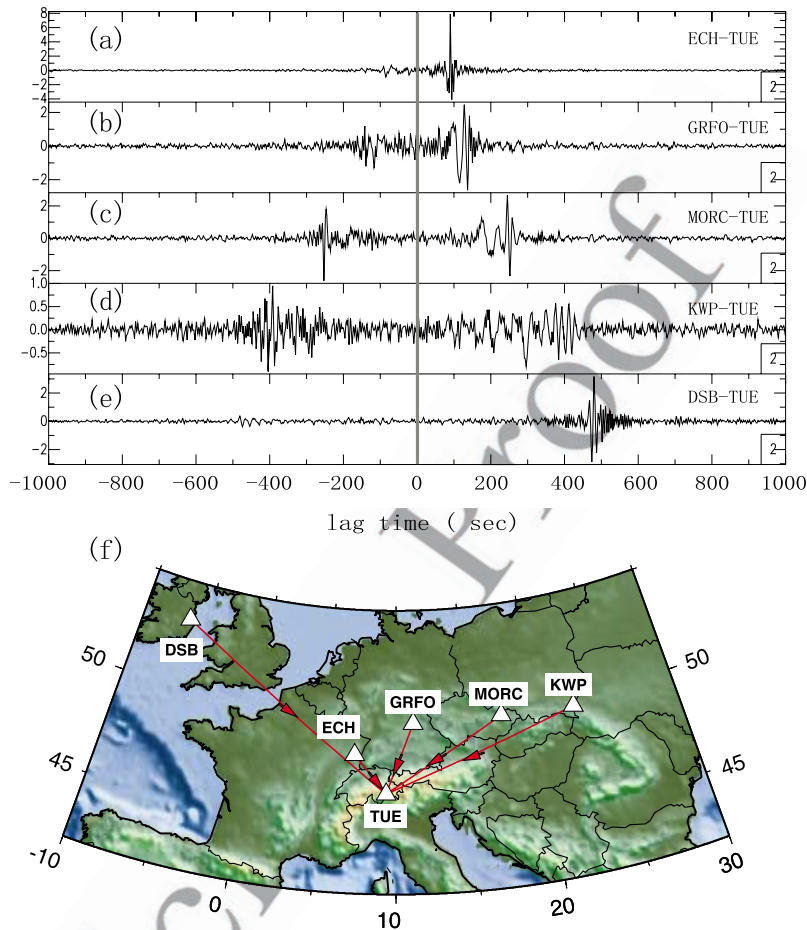


Figure 2. (a–e) Examples of 12-month broadband cross correlations. The bold gray line indicates the zero arrival time. Cross correlations are ordered by interstation distances with station names indicated in each waveform panel. Note that the cross correlations are often asymmetric. (f) Locations of the stations (white triangles) and path segments for the corresponding cross correlations, with arrows marking the incoming directions of noise contributing to the positive components.

311 the next section for Europe and then in subsequent
312 sections for elsewhere in the world.

313 [12] To evaluate the quality and amplitude of the
314 cross correlations quantitatively, we calculate the
315 period-dependent signal-to-noise (SNR) for
316 the positive and negative components of each cross
317 correlation. SNR is defined as the ratio of the peak
318 amplitude within a time window containing the
319 surface wave signals to the root-mean-square of the
320 noise trailing the signal arrival window. The signal
321 window is determined using the arrival times of
322 Rayleigh waves at the minimum and maximum
323 periods of the chosen period band (6 to 50 s) using
324 the global 3-D shear velocity model of *Shapiro and*
325 *Ritzwoller* [2002]. The period dependence of SNR
326 is determined by applying a series of narrow band-
327 pass (ranging from 5 to 10 mHz) filters centered
328 on a grid of periods from 6 to 50 s. Figure 4a

shows an example of a positive component broad- 329
band cross correlation (eighth panel) along with 330
seven narrow band-pass filtered time series. 331
Rayleigh wave signals show up clearly in each of 332
these bands. Figure 4b displays the corresponding 333
SNR as a function of period. SNR in this example 334
(and generally) peaks in the primary microseism 335
band (10–20 s), around 14 s period. 336

[13] We use SNR as a proxy to estimate the 337
strength of noise sources, which is similar to the 338
normalized amplitude used by *Stehly et al.* [2006] 339
to estimate noise strength because the root-mean- 340
square of the noise trailing the signal arrival is 341
similar for the cross correlations within the same 342
seismic array. For each cross correlation, we have 343
two SNR measurements for positive and negative 344
components, respectively, to indicate the noise 345
flux from the two opposite directions along 346

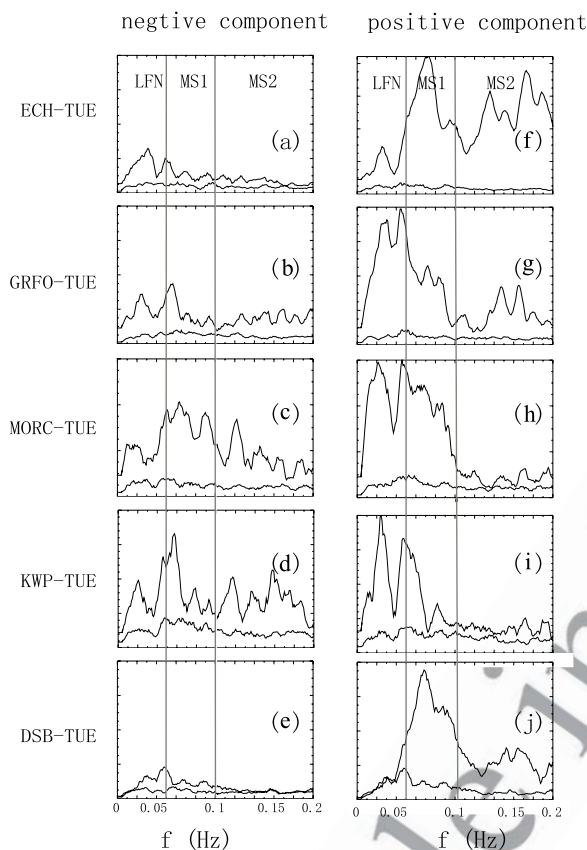


Figure 3. Normalized spectra of (a–e) negative and (f–j) positive components of the cross correlations shown in Figure 2. The three frequency bands of LFN, MS1 and MS2 delineated by the bold lines correspond to the infragravity band and the primary and secondary microseism bands.

347 the great circle linking the stations. Combining all
348 the cross correlations within a seismic array, we
349 can estimate noise energy flux from all azimuthal
350 directions. Since we do normalization in both the
351 time and spectral domain on continuous noise time
352 series before performing cross correlations, the
353 estimate of noise strength from SNR can only tell
354 us the relative strength as a function of azimuth.

355 3. Sources of Ambient Noise Observed 356 in Europe

357 [14] To investigate the directions of the incoming
358 ambient noise systematically, we plot in Figure 5
359 the azimuthal distribution of SNR for the positive
360 and negative components of each cross correlation
361 at 8, 14, 25 and 50 s period in the northern winter
362 and northern summer of 2004. Each line points in
363 the direction from which the energy arrives (i.e., it
364 points to the source location) and its length is

proportional to the SNR. At 8 and 14 s period, 365
lines drawn to the edge of circle represent a SNR of 366
at least 80, and at 25 s and 50 s the lines to the 367
circle's edge mean the SNR is at least 60. 368

[15] The periods of 8 and 14 s are near the center of 369
the secondary (5–10 s) and primary (10–20 s) 370
microseism bands, respectively. The strength and 371
directionality of ambient noise at these two periods 372
are shown in Figure 5 to be very similar to one 373
another, and they demonstrate similar, strong sea- 374
sonal dependence with much stronger noise arriv- 375
ing in the northern winter than in the northern 376
summer. The seasonal variation in the strength of 377
ambient noise, with the noise level being much 378
higher in winter than in summer, is consistent with 379
higher sea states in winter than in summer in the 380
north Atlantic [Webb, 1998]. In the winter, at both 381
periods the strongest energy is arriving from the 382
northwest quadrant. The strongest arrivals are also 383
from the northwest quadrant during the summer, 384
but the arrivals from the north are less energetic. 385
The one exceptional difference between the pat- 386
terns of energy arrival at 8 and 14 s is stronger 387
noise from the northeast quadrant at 14 s period 388
during the northern summer. 389

[16] The patterns of energy arriving at the longer 390
periods of 25 and 50 s are quite distinct from waves 391
in the microseism band. These waves display little 392
seasonal variability and the azimuthal patterns of 393
energy arriving at these periods are very similar to 394
one another, with the strongest energy arriving 395
from the northeast at both periods and seasons. 396
The only appreciable difference between 25 and 397
50 s is that the SNR at 25 s is higher than at 50 s 398
period. 399

[17] Figures 6 and 7 illustrate possible source 400
locations by back-projecting along a great circle 401
arc for each station pair with a SNR > 20. In the 402
secondary microseism band (~8 s period) shown in 403
Figure 6, source directions are broadly distributed 404
to the west and northwest of Europe. In our view, 405
the simplest distribution of source locations would 406
be for them to occur near the European coast, 407
ranging from west of Spain to the European Arctic 408
coast of the Baltic peninsula in winter. The alter- 409
native would be for the sources to emanate from a 410
much larger area, to lie in deep water spanning the 411
entire North and Central Atlantic. We view this as 412
implausible. In northern summer, the range of 413
azimuths for the high SNR sources diminishes to 414
near coastal France, England, the North Sea region, 415
and coastal Norway. At 14 s period during the 416
summer, seismic energy also arrives to the Euro- 417

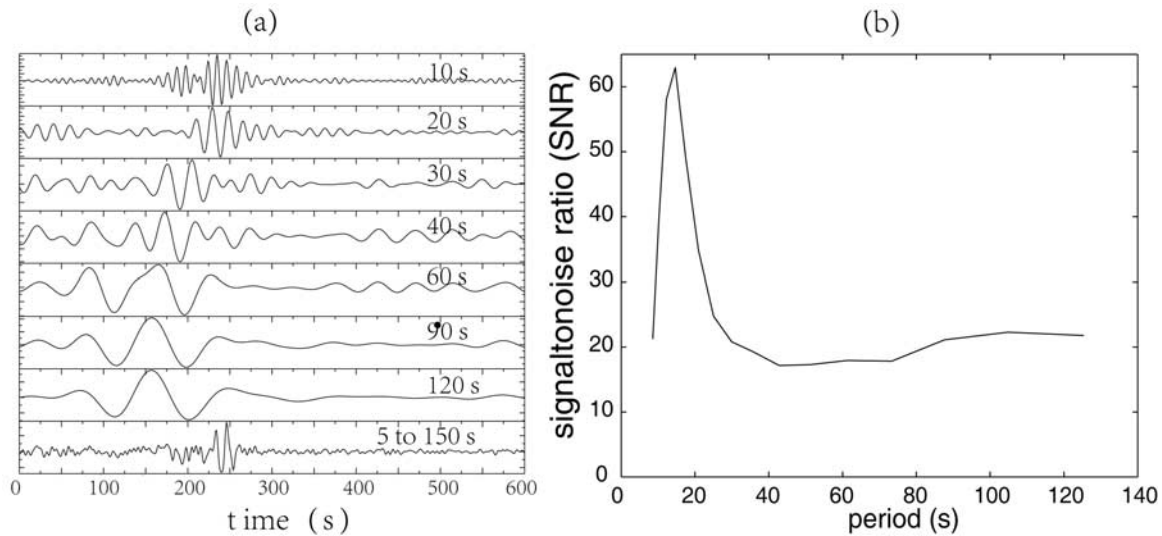


Figure 4. (a) Example of a broadband positive component cross correlation using 12 months of data between stations IBBN (Ibbenbueren, Germany) and MOA (Molln, Austria). The broadband signal (5–150 s) is shown in the eighth panel. Other panels are narrow band-pass filtered waveforms with the central periods indicated in each panel. (b) Calculated SNR values from each narrow band-passed filtered waveforms versus period.

418 pean stations from the northeast, apparently having
419 emanated from east of Asia. Again, the simplest
420 explanation would be for the sources to occur along
421 the east Asian coastline, predominantly off of China,
422 Korea/Japan, and Russia. The sole significant dif-
423 ference between 8 and 14 s period is these arrivals
424 from the east Asian coast at 14 s during the northern
425 summer. This can be understood as a wave propa-
426 gation phenomenon, with the 8 s waves having
427 been attenuated more than those at 14 s. Similarly,
428 east Asian earthquake waves observed in Europe
429 are enriched at 14 s relative to 8 s wave energy. The
430 8 s Rayleigh waves similarly cannot propagate
431 coherently over transcontinental distances.

432 [18] At 25 s and 50 s, illustrated in Figure 7, the
433 patterns of the back-projected rays are nearly
434 identical with each other in summer and winter.
435 The strongest arriving energy is from the northeast,
436 probably having originated along the western
437 Pacific rim. Again, we view the shallow water
438 source location to be more plausible than the deep
439 water sources distributed over a much larger area.
440 There are fewer large amplitude arrivals from the
441 western quadrants. Those that exist probably have
442 originated near the European coast from the same
443 reason. Although deep water sources for the longer-
444 period arrivals cannot be ruled out on the basis
445 of the seismic evidence alone, the spatial distribu-
446 tion of sources would have to be very diffuse and
447 we are unaware of any evidence for this.

[19] Our analysis of ambient noise directionality in 448
Europe indicates little significant difference between 449
the directional content of energy arriving in the two 450
microseism bands. The differences that do exist can 451
be attributed to the fact that the longer-period 452
primary microseismic energy (~14 s) propagates 453
farther than secondary microseismic energy (~8 s), 454
and therefore can arise from the Pacific rim of 455
Asia. In addition, the principle of simplicity argues 456
for concentrated near-coastal source locations as 457
opposed to diffuse mid-oceanic source locations 458
over a much larger area. However, the method we 459
use cannot locate noise sources unambiguously, 460
and the results in Europe may differ from those 461
elsewhere in the world. Thus, in the following 462
sections, we analyze ambient noise directionality 463
in southern Africa, Tibet, and North America. 464

4. Further Analysis: Cross Correlations of Ambient Noise in Southern Africa and Asia 465 466 467

[20] The stations used in this analysis are shown in 468
Figure 8. Twelve months of data are processed 469
using stations from two PASSCAL experiments; 470
the Southern Africa Seismic Experiment (SASE) 471
with data from 1998 and the Eastern Syntaxis Tibet 472
Experiment with data from 2003 and 2004. We 473
process data exactly as for the European stations, 474
but obtain results only at periods of 8, 14 and 25 s 475
because the arrays are smaller and longer-period 476

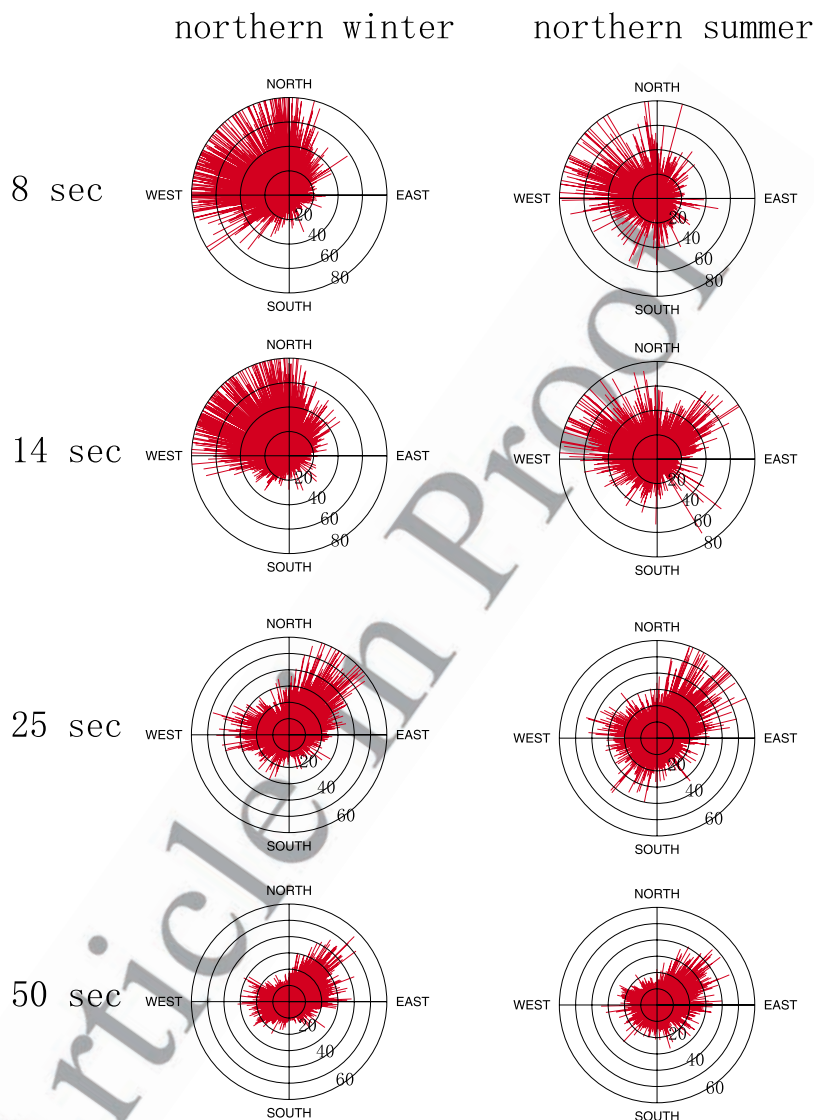


Figure 5. Azimuthal distribution of SNR of 5-month stacks during the (left) northern winter and (right) summer at periods 8, 14, 25 and 50 s taken from European seismic stations. SNR levels are indicated by the concentric circles with values shown in each of the diagrams.

477 results are less robust than in Europe. The azi-
478 muthal distribution of SNR from the southern
479 African, Tibetan, and European stations are plotted
480 in Figure 9 in both the northern summer and
481 winter.

482 [21] Like in Europe, at 8 and 14 s period, consid-
483 erable seasonal variability is observed both in
484 southern Africa and Tibet. In Tibet, ambient noise
485 is stronger in the northern winter than the northern
486 summer and the principal directions of noise swing
487 to the south in the northern summer. In understand-
488 able contrast to the observations in Europe, however,
489 ambient noise is stronger at these periods in south-
490 ern Africa during the northern summer (southern

winter) than in the northern winter (southern sum- 491
mer) (Figures 9a–9d). Thus, at 8 and 14 s period, 492
ambient noise is stronger in the local winter in most 493
directions in all three locations. In southern Africa, 494
the azimuthal content of noise emanating from the 495
southern quadrants at these two periods is very 496
similar to one another and there is less seasonal 497
dependence. The simplest explanation is that ambi- 498
ent noise from the southern quadrants arrives 499
from nearby coastlines having been generated 500
there. Noise from the northern quadrants in south- 501
ern Africa is different at 8 and 14 s, however, and 502
there is a stronger seasonal dependence. Strong 503
noise (SNR > 40) at 14 s arriving from the north 504
and northwest to southern Africa during the north- 505

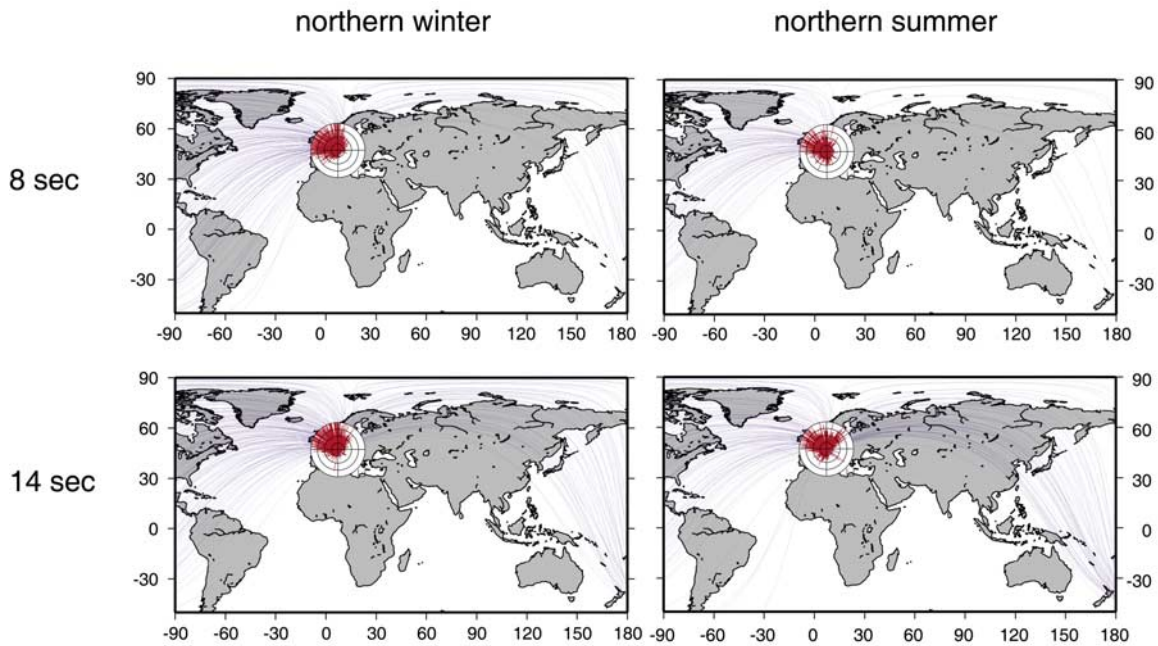


Figure 6. Back-projected great circle paths of cross correlations at periods of 8 and 14 s in the northern summer and winter with corresponding azimuthal distribution overlotted at the center of Europe. The great circle paths indicate the approximate locations along which noise sources constructively contribute to surface wave signals. Paths shown here have SNR > 20.

506 ern winter, back-projects to the northern European
507 coasts, similar to observations in Europe. Strong
508 noise (SNR > 60) arriving at 14 s from the
509 northeast, which is particularly strong in the north-

ern summer, is more difficult to interpret. For 510
example, as shown in Figure 9d, this noise back- 511
projects to the east Asian coast similar to results 512
from the European stations, but the Tibetan results 513

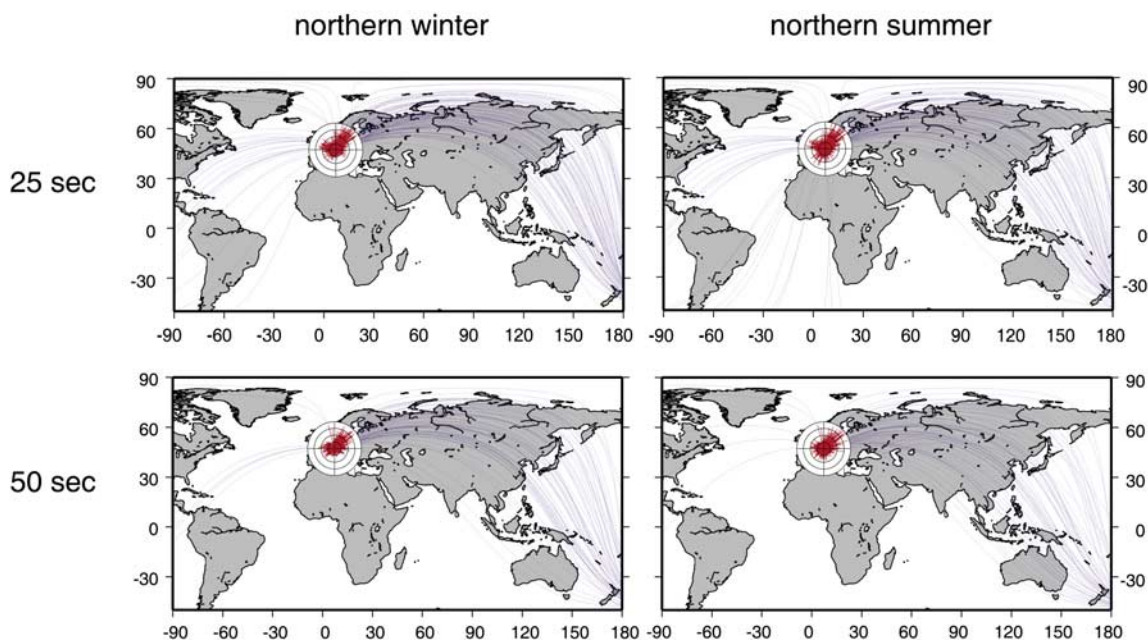


Figure 7. Same as Figure 6 but for periods of 25 and 50 s.

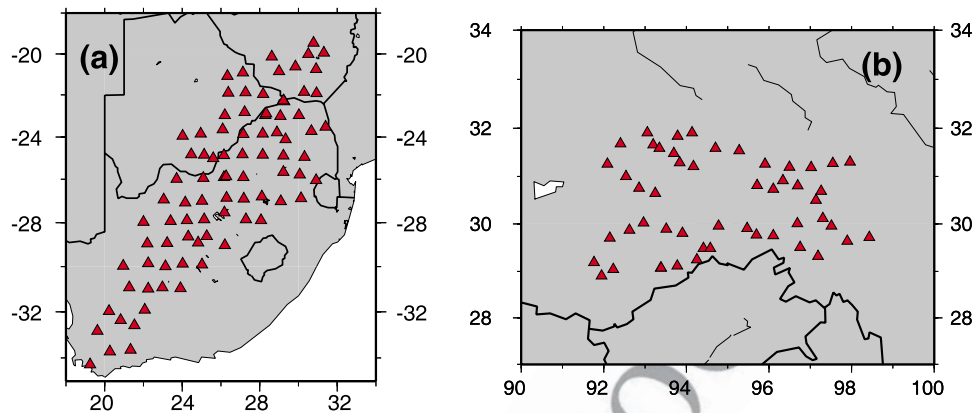


Figure 8. Stations used in southern Africa from the Southern African Seismic Experiment and Tibet from the Eastern Syntaxis Tibet Experiment.

514 indicate that the strongest noise there is coming
515 from the southwest rather than the northeast. It is
516 unlikely, therefore, that the strong arrivals at 14 s
517 observed at the European and southern African
518 stations emanate from a single source region in
519 east Asia. We believe that it is more likely that the
520 14 s southern African energy finds its source near
521 the African coast or perhaps along the coastlines of
522 the Arabian Sea.

523 [22] These observations illustrate that the azimuthal
524 patterns of microseismic energy arriving at these
525 three locations display some common systematics,
526 particularly as related to seasonal variability. Dif-
527 ferences between the 8 s and 14 s observations
528 again can be understood largely as propagation
529 effects. The source locations of the noise arriving
530 in these regions are largely distinct, however. It is,
531 therefore, unlikely that large storms in the deep
532 oceans are the direct source of microseismic energy
533 at 14 s period, which is more likely to have been
534 produced in relatively shallow near coastal waters.
535 The seasonal variability of the microseisms, how-
536 ever, illustrates that large deep ocean storms are
537 probably the cause of the ocean gravity wave
538 energy that transforms to ambient seismic noise
539 in shallow waters.

540 [23] At 25 s period, as in Europe, there is little
541 seasonal dependence of the directionality of ambi-
542 ent noise in southern Africa and the azimuthal
543 content of ambient noise at this period differs
544 substantially with that at either 8 s or 14 s period.
545 The southern African noise at this period is gener-
546 ally of larger amplitude than in Europe, probably
547 because of higher sea states in the Southern Hemi-
548 sphere, and is also more omnidirectional than in
549 Europe, consistent with the source of the ambient
550 noise occurring near the coast along much of
551 southern Africa rather than in deep water to the

south of Africa where sea states are highest. In 552
Tibet, like Europe and southern Africa, the azi- 553
muthal distribution of incoming noise at 25 s 554
differs substantially from 8 or 14 s period. How- 555
ever, unlike Europe or southern Africa, there is 556
substantial seasonal variability, with strong noise 557
coming from the southern quadrants in both the 558
northern summer and winter but also from the 559
north in the northern winter. The directions of 560
arrival of strong noise in Europe, southern Africa, 561
and Tibet at 25 s are not consistent with a single or 562
small number of exceptionally strong source loca- 563
tions, but rather indicate that strong noise emerges 564
at these arrays from many directions, presumably 565
with a broad distribution of source locations. These 566
observations are, therefore, at variance with a deep 567
water source for ambient noise at 25 s period. 568

5. Further Analysis: Cross Correlations of Ambient Noise in North America

571 [24] We also use continuous seismic data from 571
numerous stations in California, the eastern United 572
States, Alaska and northwest Canada, processing 573
them using the same methods as for the European, 574
southern African, and Tibetan data. The stations 575
are shown in Figure 10 and the results are pre- 576
sented at 8, 14, and 25 s in Figure 11. 577

578 [25] At 8 and 14 s period, results for the stations in 578
the eastern United States and Alaska/Canada are 579
straightforward. SNR is larger in the northern 580
winter than the northern summer, but the directional 581
dependence of noise is largely seasonally indepen- 582
dent. In addition, the directional patterns at these 583
periods are largely similar. In Alaska/northern 584
Canada, ambient noise at these periods arrives 585
mainly from the south, presumably along the 586
Pacific coast of Canada and Alaska. In the eastern 587

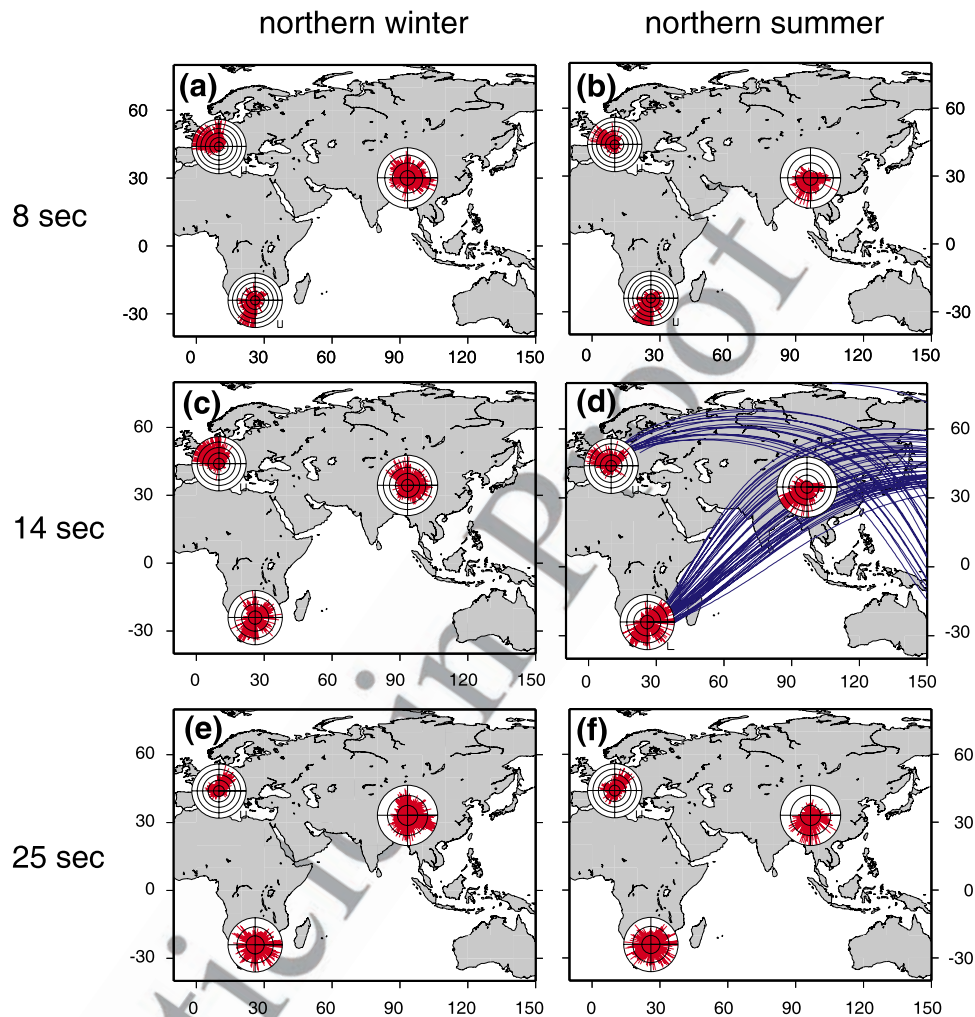


Figure 9. Similar to Figure 6 but here the azimuthal distribution of SNR of 5-month stacks at periods (a and b) 8, (c and d) 14, and (e and f) 25 s in southern Africa and Tibet during the northern winter (Figures 9a, 9c, and 9e) and summer (Figures 9b, 9d, and 9f) are compared with results from Europe. SNR levels in each region are indicated by the concentric circles that are scaled in multiples of 20. Paths in Figure 9d are back-projected great circle curves with SNR > 60.

588 United States, in contrast, ambient noise arrives
589 mainly from the northeast and west, i.e., either
590 from the Canadian Atlantic coast or the Pacific
591 coast of North America. Thus, at these locations
592 there is no evidence of significant differences in the
593 source locations at 8 and 14 s period.

594 [26] In the microseismic bands in California, the
595 results are somewhat more complicated, however.
596 At 8 s, there is weak seasonal variability with
597 stronger waves arriving from the northwest in
598 winter than in summer. At 14 s, the seasonal
599 variation is strong and the 8 s and 14 s azimuthal
600 patterns differ from one another. In the northern
601 winter, the strongest signals arrive to California
602 from the northwest and northeast at 14 s, presu-
603 mably arriving from the northern Pacific and north-

ern Atlantic coasts of North America. In the 604
northern summer, however, the strongest arrivals 605
are from the south and southwest, with the source 606
locations probably being localized to the nearby 607
coasts. These patterns are different from those at 8 s 608
period, in which the dominant arrivals are in the 609
southwest quadrant throughout the year, similar to 610
the azimuthal distribution at 14 s period during the 611
northern summer. *Stehly et al.* [2006] argue from a 612
similar observation for the physical decoupling of 613
the primary and secondary microseisms. Consistent 614
with our observations in other regions, we believe 615
the explanation is that these arrivals at 14 s period 616
are coming from North American coastlines in the 617
north Pacific and north Atlantic which are too far 618
to be observed well at 8 s period. 619

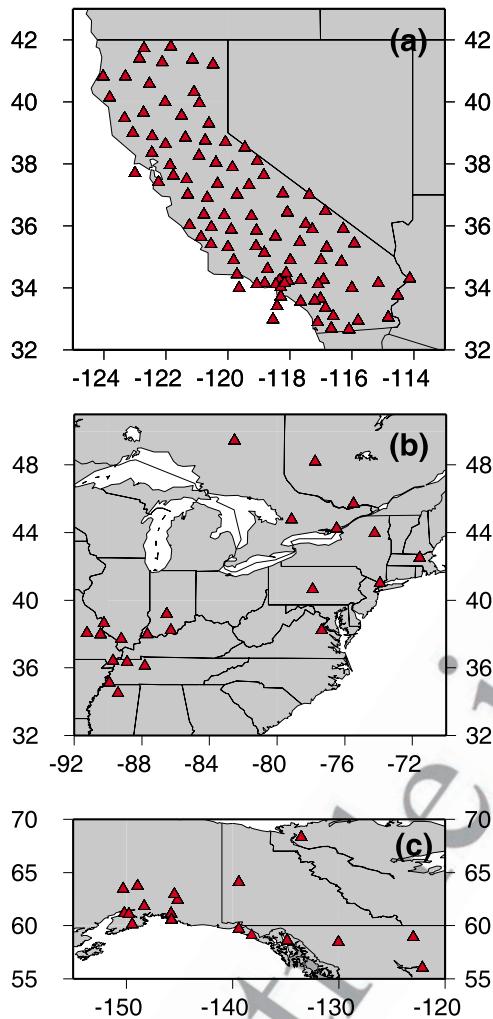


Figure 10. Stations used in North America.

620 [27] At 25 s period across North America, the
621 azimuthal patterns are largely seasonally invariant
622 with the most energetic waves apparently coming
623 from the Pacific coast of the western United States.

624 [28] Thus, from microseismic band to longer-
625 period ambient noise in North America, these
626 results are consistent with near-coastal sources
627 similar to our observations in the Eastern Hemi-
628 sphere. The observed differences in directivity at 8,
629 14 and 25 s can be attributed to propagation and
630 attenuation, rather than the location of generation.

631 6. Azimuthal Coverage and Recovery 632 of Empirical Green's Functions

633 [29] In most theoretical treatments of ambient noise
634 tomography and coda wave interferometry, the
635 assumption of a perfectly homogeneous azimuthal

distribution of noise sources is made [e.g., *Snieder*, 636
2004]. The observed distribution of ambient noise 637
is far from homogeneous, however, with excep- 638
tionally strong signals sometimes emanating only 639
from a narrow range of azimuths. Therefore ques- 640
tions have been raised [e.g., *Rhie and Romanowicz*, 641
2006] about the effect that this will have on the 642
emergence of accurate empirical Green's functions 643
from cross correlations of ambient noise and 644
whether the observations can be used meaningfully 645
to obtain dispersion measurements and perform 646
tomography. 647

[30] This question has been addressed observation- 648
ally in previous studies [e.g., *Shapiro et al.*, 2005; 649
Yang et al., 2007; *Lin et al.*, 2008; *Moschetti et al.*, 650
2007; *Bensen et al.*, 2007a, 2007b] using several 651
lines of evidence. These studies showed that the 652
observed interstation empirical Green's functions 653
are similar to earthquake signals when earthquakes 654
occur near to one of the stations, that dispersion 655
curves are seasonally repeatable even though ambi- 656
ent noise characteristics may change substantially, 657
and that the dispersion curves are consistent with 658
one another even when azimuths are quite differ- 659
ent. In addition, they showed that the resulting 660
group and phase velocity maps reproduce geolog- 661
ical structures faithfully. These and other reasons 662
help to establish the veracity of ambient noise 663
tomography. It should be borne in mind, however, 664
that considerable efforts are exerted in processing 665
ambient noise data to identify bad measurements 666
(commonly more than half of all observations), 667
some of which result from low signal levels or 668
incomplete constructive/destruction interference in 669
the generation of the observed Green's functions. 670

[31] The established veracity of ambient noise 671
tomography appears, however, to be in conflict with 672
the existence of relatively narrow azimuthal ranges 673
with extraordinarily large amplitudes of ambient 674
noise (e.g., Figures 12a–12c). Figures 12d–12f, 675
which presents histograms of the number of 676
12-month European interstation cross correlations 677
with SNR > 10 on either the positive or negative 678
component, illustrates why this is not contradictory. 679
The reason is that signals with SNR > 10 emerge 680
from a wide range of azimuths. Only the very 681
strongest signals are azimuthally limited. Thus, 682
although there are preferred directions for ambient 683
noise, predominantly at very short periods, signif- 684
icant ambient noise signals exist at a wide range of 685
azimuths. The reason for this can be understood in 686
terms of the interpretation that ambient seismic 687
noise is generated in shallow near coastal water. 688

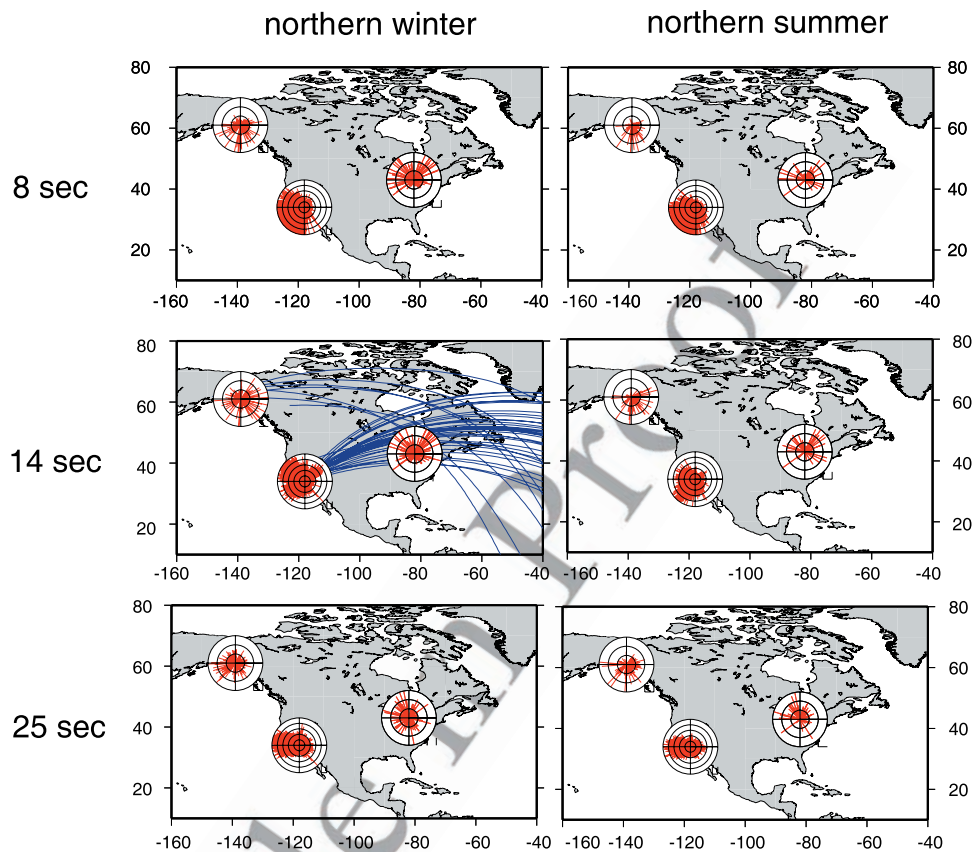


Figure 11. Same as Figure 6 but for stations in the North America: California, the eastern United States, and Alaska/Canada.

689 [32] In order to demonstrate that accurate empirical
690 Green's functions are obtained from long time
691 noise series when ambient noise sources have an
692 inhomogeneous azimuthal distribution with strong
693 sources in some preferential directions, we present
694 four synthetic experiments with different noise
695 energy distributions. Synthetic sources are randomly
696 distributed in a circular region with a diameter of
697 4000 km and a pair of stations are placed 450 km
698 apart (Figure 13a). Each synthetic source emits a
699 wavelet at a random initial time and at a random
700 location with frequency content dominantly between
701 about 15 and 25 s period. The waveform of the
702 wavelet is the second derivative of a Gaussian
703 function with a 20 s standard deviation. The wave
704 velocity inside the circular region is 3 km/s every-
705 where. For each experiment, we run 30 simulations
706 for each individual day totaling 30 d. For each day,
707 6000 sources are randomly distributed, but source
708 energy has an azimuth-dependent distribution as
709 shown in Figures 13b–13e. The resulting cross
710 correlations are 30-d stacks. The empirical Green's
711 functions, which are the negative time derivatives

of the resulting cross correlations [Snieder, 2004],
are plotted in Figure 14a with the theoretical
Green's function plotted at the bottom as compar-
ison. The resulting SNR for the simulations is
similar to empirical Green's functions obtained
for real data.

[33] In experiment I, the distribution of sources is
azimuthally homogenous. Thus the cross correla-
tion is nearly symmetric. In experiment II, there is
stronger source energy coming from the right,
which makes the cross correlations highly asym-
metric with a much higher signal-noise-ratio on the
positive component. In experiment III, stronger
source energy comes from the northeast direction,
similar to the incoming directions observed in
Europe at 30 s period (Figure 12c) for stations
oriented west-east. The resulting cross correlation
is nearly symmetric because the strong sources from
the northeast interfere with each other *destructively*.
In experiment IV, stronger source energy comes
from the forth quadrant, which resembles the
source distribution we observe at periods of 8 and
14 s in Europe (Figure 12a). The resulting cross

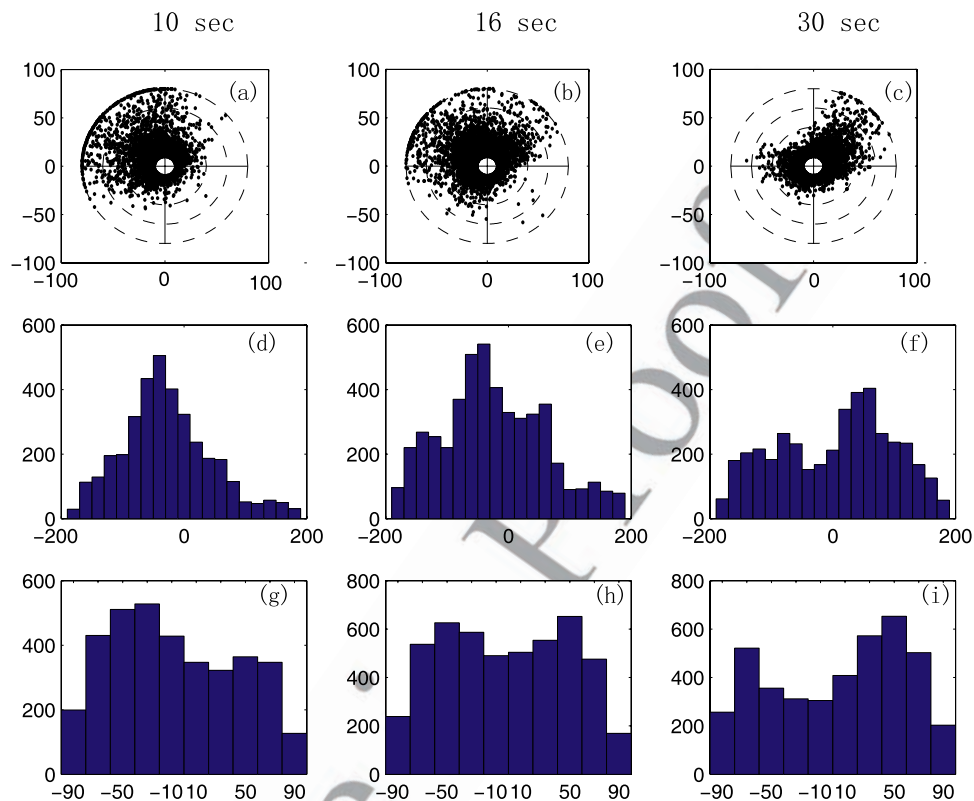


Figure 12. (top) Azimuthal distributions and (middle) histograms of the incoming directions of ambient noise. SNR levels are indicated by dashed concentrated circles with values denoted. (bottom) Histograms of bearing angles for cross correlations with SNR > 10 at 10, 16 and 30 s. Bearing angles are defined as the angle between the orientation of a path segment and the northern direction.

735 correlation is asymmetric with a much higher
736 signal-noise-ratio on the negative component.
737 Arrival times of the peak energy at both positive
738 and negative lags of the four cross correlations
739 are about 150 s, which is the actual time for the wave
740 to propagate between the two stations. We follow
741 *Lin et al.* [2008] and obtain phase velocity mea-
742 surements for the retrieved cross correlations by
743 automatic frequency-time analysis (FTAN). The
744 measured phase velocities and travel times are
745 close to the input phase velocity (3 km/s) and
746 travel time (150 s) with error less than about
747 0.5% at all periods (Figures 14b and 14c). The
748 maximum travel time error ($<2/3$ s) is less than
749 measurements errors with real data and consider-
750 ably less than the RMS of data misfit in ambient
751 noise phase velocity tomography [e.g., *Lin et al.*,
752 2008, Yang et al., submitted manuscript, 2007].

753 [34] These four synthetic experiments show that if
754 ambient noise exists over a broad azimuthal range
755 even at relatively low levels, accurate empirical
756 Green's functions will emerge from long time
757 series of the ambient noise even when the distri-

bution is far from azimuthally homogenous. We
758 have also conducted numerical experiments with
759 random sources confined to an annulus with the
760 radius of the inner circle equal to one fourth of the
761 radius of the outer circle. The source azimuthal
762 distributions for these experiments are the same as
763 those shown in Figures 13b–13e. These experi-
764 ments resemble the circumstances that the loca-
765 tions of ambient noise are distant relative to
766 seismic stations. The results from these numerical
767 experiments are almost identical, respectively, to
768 those four cases shown in Figure 13. These
769 numerical experiments imply that the resulting
770 cross correlations of ambient noise are determined
771 by the relative azimuthal distributions rather than
772 detailed lateral distributions of sources. 773

[35] With the results from the synthetic experi-
774 ments in mind, Figures 12g–12i provide additional
775 insight into why ambient noise tomography works
776 so well. It presents bearing angles of path segments
777 for the selected cross correlations at periods of 10,
778 16 and 30 s. Bearing angles are defined as the
779 angle between the orientation of a path segment
780

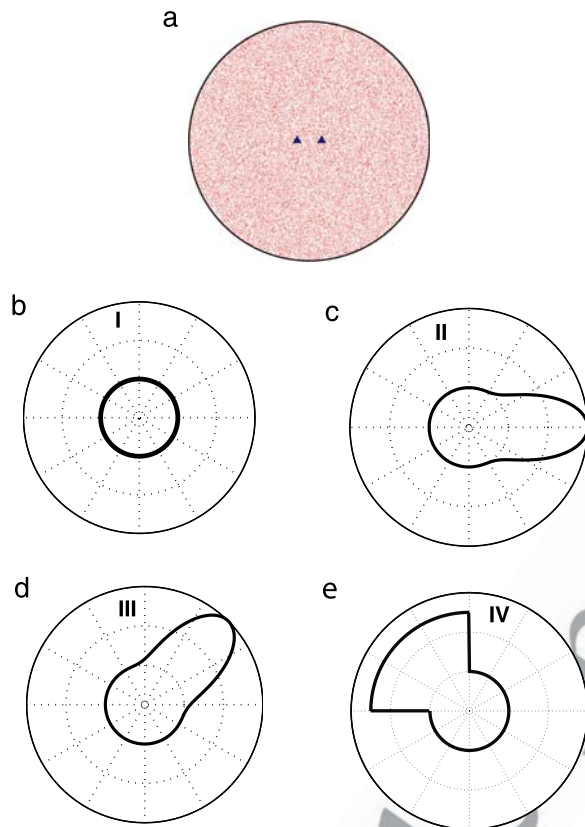


Figure 13. (a) Circular region with a diameter of 4000 km for the noise simulation. Each red dot represents a randomly distributed source. The two blue triangles are the two receiver stations placed 450 km apart. (b–e) Azimuthal distributions of the strength of source energy delineated by the bold lines for experiments I, II, III, and IV, respectively.

781 and the northern direction with a range between
782 -90° and 90° because, for any cross correlation,
783 positive and negative components with noise coming
784 from two opposite directions have the same
785 orientation. Although there is a slight preponderance
786 of paths striking northwest-southeast across
787 Europe, particularly at short periods, the distribution
788 is strikingly homogeneous, which is good for
789 the emergence of accurate empirical Green's functions
790 and for resolution in surface wave tomography,
791 particularly for extracting information about
792 azimuthal anisotropy. These observations provide
793 another line of evidence that highlights the advantage
794 of ambient noise in providing homogenous ray
795 coverage in surface wave tomography.

796 7. Conclusions

797 [36] Three principal questions have motivated this
798 study. (1) Does the directivity of ambient noise

provide evidence that the primary and secondary 799
microseisms are physically decoupled? (2) Is 800
ocean-produced ambient seismic noise generated 801
in relatively shallow near-coastal waters or in deep 802
water at longer periods? (3) Is the azimuthal 803
distribution of ambient noise sufficiently homoge- 804
neous to allow for the retrieval of largely unbiased 805
empirical Green's functions? We addressed each of 806
these questions by investigating the strength and 807
azimuthal distribution of ambient noise between 808
8 and 50 s period in Europe, southern Africa, Tibet, 809
and three regions in North America (California, 810
Alaska/northern Canada, eastern United States). 811
Because the methods we use recover information 812
only about the direction to strong ambient noise 813
sources and not their absolute locations, the results 814
are not entirely unambiguous. The inferences that 815
we draw, therefore, are based also on appealing to 816
the principle of simplicity. 817

[37] First, we find no compelling evidence for 818
difference in source locations of the primary and 819
secondary microseisms. The seasonal variation of 820
the two microseisms is similar in all regions that 821
we studied. Although the azimuthal distributions of 822
the two microseisms do vary in some places, this 823
difference is most simply attributable to the fact 824
that the primary microseismic wave can propagate 825
coherently over much longer distances than the 826
secondary microseismic wave. It is possible and 827
probably likely, however, that the relative ampli- 828
tude of the primary and secondary microseisms 829
upon generation of these waves is globally vari- 830
able. However, characterizing the regional varia- 831
tion of this ratio is beyond the scope of this paper. 832

[38] Second, in all studied regions and at all 833
periods studied here (8–50 s) the most simple 834
location for the source of ambient noise lies in 835
near-coastal waters. Deep water sources cannot be 836
formally ruled out by the methods we apply here. 837
We show, however, that deep water source regions 838
would have to cover much of the ocean basins, 839
which we argue is unlikely. In addition, source 840
directivity at long periods on different continents 841
differs, and, therefore, there is no evidence for 842
common source locations in deep water. 843

[39] Third, and perhaps surprisingly, ambient noise 844
emerges in each of the studied regions at a broad 845
range of azimuths. If this does appear surprising it 846
is probably because studies of ambient noise typ- 847
ically have focused on characterizing the strongest 848
ambient noise directions, which are limited in 849
azimuth. Even though the strongest noise emerges 850
only from a few directions in most places, strong 851

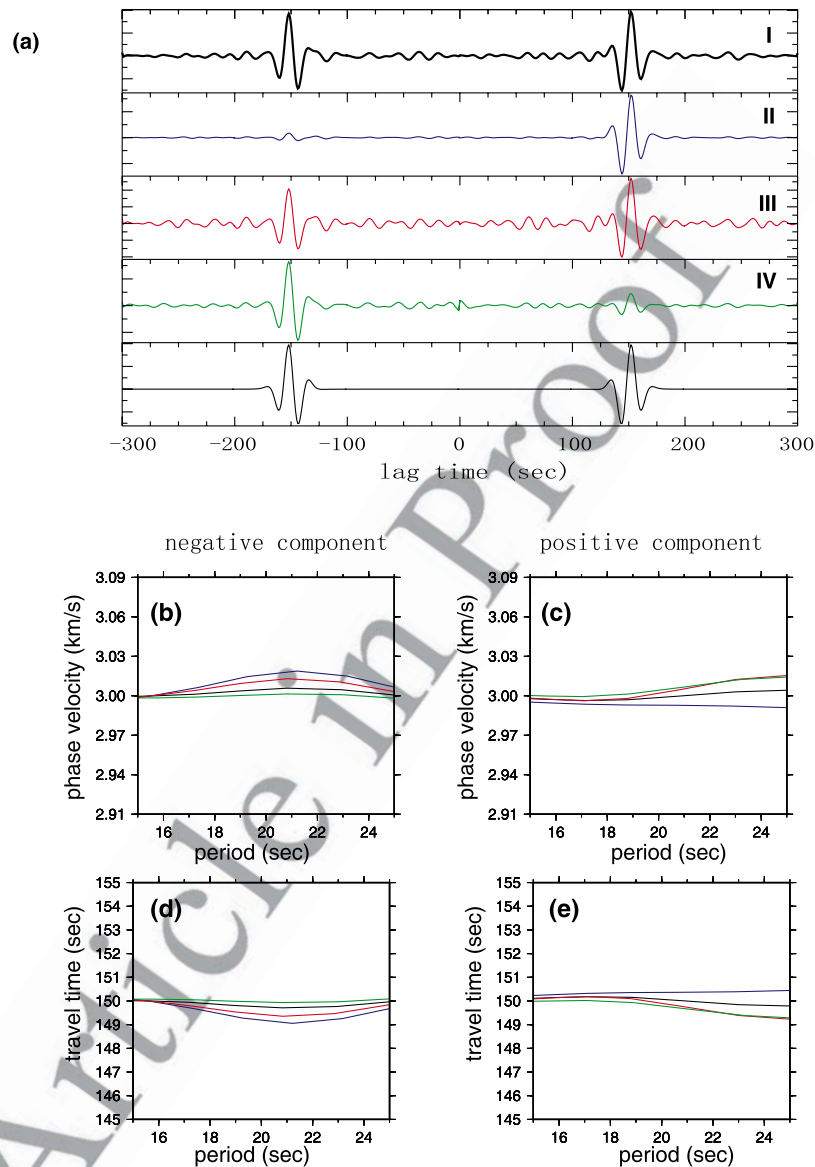


Figure 14. (a) Normalized empirical Green's functions (EGFs) from synthetic cross correlations for experiments I, II, III, and IV. At bottom is the theoretical Green's function. (b and c) Phase velocity measurements obtained on the normalized EGFs for negative and positive components, respectively. (d and e) Travel times at various periods for EGFs. The black line is for experiment I, the blue line is for experiment II, the red line is for experiment III and the green line is for experiment IV. Input phase velocity is 3 km/s, and travel time is 150 s.

852 ambient noise emerges from many directions.
853 Thus, for the orientation of most station pairs,
854 sufficiently strong ambient noise is present to be
855 the basis for the retrieval of reliable empirical
856 Green's functions. Nevertheless, there are some
857 azimuths in most regions where ambient noise is
858 so weak that interstation cross correlations will not
859 provide a good empirical Green's function. From a
860 practical perspective, therefore, these cross correla-
861 tions have to be identified and removed as
862 candidate empirical Green's functions. Typically,

these cross correlations have a low signal-to-noise 863
ratio, and SNR is useful in the data processing part 864
of ambient noise tomography to identify the accept- 865
able empirical Green's functions [e.g., *Bensen et* 866
al., 2007a]. The principal caveat is that there are 867
some exceptionally strong spurious signals, such as 868
the persistent 26 s resonance in the Gulf of Guinea 869
[*Shapiro et al.*, 2006], that require dedicated data 870
processing to remove [*Bensen et al.*, 2007a]. 871

[40] In closing, the ways in which the strength and 872
distribution of ambient noise vary in both azimuth 873



874 and region appear to be consistent generally with
875 the hypothesized generation of ambient noise
876 advocated by *Rhie and Romanowicz* [2006]. In
877 this scenario, wind energy is converted to ocean
878 wave energy in the deep oceans. Ocean wave
879 energy is then transported to the fringes of
880 continents as ocean gravity waves (or so-called
881 infragravity waves at longer periods). Near
882 coastlines, ocean gravity waves convert to solid
883 earth propagating seismic waves when water is
884 shallow enough to allow their direct interaction
885 with the seafloor. The primary and secondary
886 microseisms are physically coupled through a
887 nonlinear, frequency-doubling process resulting
888 from wave-wave interactions between the direct
889 and coastally reflected waves.

890 [41] It may not be generally appreciated that this
891 mechanism would predict that ambient noise is
892 well distributed in azimuth. Ocean gravity waves
893 generated in deep water will propagate to coast-
894 lines broadly across the ocean basin where seismic
895 waves will be generated over a large area in
896 relatively shallow water. This mechanism also
897 would predict that the strongest seismic waves
898 would be generated when and where the storm
899 intersects the coastline. Both of these predictions,
900 the broad area of generation of ambient noise along
901 coastlines and the strongest waves emanating from
902 only a few azimuths, are consistent with our
903 observations. Given the ambiguities inherent in
904 the methods applied herein, however, we view
905 these results as relatively weak confirmation of the
906 hypothesized mechanism of *Rhie and Romanowicz*.
907 More direct observations are needed to test this
908 hypothesis further.

909 Acknowledgments

910 [42] The data used in this research were downloaded from
911 continuous ftp database of the Orfeus (Observatories and
912 Research Facilities for European Seismology) Data Center
913 and from the IRIS Data Management Center. The authors
914 are deeply grateful to the networks that contribute data to the
915 Virtual European Broadband Seismic Network (VEBSN), a
916 partnership of more than 30 local, regional and global arrays
917 and networks. In addition, the authors would like to acknowl-
918 edge two PASSCAL experiments that provided data for this
919 research: the Southern Africa Seismic Experiment and the
920 Eastern Syntaxis Tibet Experiment. The authors gratefully
921 acknowledge Barbara Romanowicz, another anonymous re-
922 viewer and Editor John Tarduno for comments that improved
923 the manuscript. This research was supported by U.S. National
924 Science Foundation grant EAR0711526 and U.S. Department
925 of Energy contract DE-FC52-2005NA26607.
926

References

- 927
- Aki, K., and B. Chouet (1975), Origin of coda waves: Source, 928
attenuation, and scattering effects, *J. Geophys. Res.*, *80*, 929
3322–3342. 930
- Bensen, G. D., M. H. Ritzwoller, M. P. Barmin, A. L. Levshin, 931
F. Lin, M. P. Moschetti, N. M. Shapiro, and Y. Yang (2007a), 932
Processing seismic ambient noise data to obtain reliable broad- 933
band surface wave dispersion measurements, *Geophys. J. Int.*, 934
169, 1239–1260, doi:10.1111/j.1365-246X.2007.03374.x. 935
- Bensen, G. D., M. H. Ritzwoller, and N. M. Shapiro (2007b), 936
Broad-band ambient noise surface wave tomography across the 937
United States, *J. Geophys. Res.*, doi:10.1029/2007JB005248, in 938
press. 939
- Cho, K. H., R. B. Herrmann, C. J. Ammon, and K. Lee (2007), 940
Imaging the upper crust of the Korean Peninsula by surface- 941
wave tomography, *Bull. Seismol. Soc. Am.*, *97*, 198–207. 942
- Derode, A., E. Larose, M. Campillo, and M. Fink (2003a), 943
How to estimate the Green's function of a heterogeneous 944
medium between two passive sensors? Application to acous- 945
tic waves, *Appl. Phys. Lett.*, *83*, 3054–3056. 946
- Derode, A., E. Larose, M. Tanter, J. de Rosny, A. Tourim, 947
M. Campillo, and M. Fink (2003b), Recovering the Green's 948
function from field-field correlations in an open scattering 949
medium, *J. Acoust. Soc. Am.*, *113*, 2973–2976. 950
- Ekstrom, G. (2001), Time domain analysis of Earth's longper- 951
iod background seismic radiation, *J. Geophys. Res.*, *106*, 952
26,483–26,493. 953
- Gudmundsson, O., A. Khan, and P. Voss (2007), Rayleigh- 954
wave group-velocity of the Icelandic crust from correlation 955
of ambient seismic noise, *Geophys. Res. Lett.*, *34*, L14314, 956
doi:10.1029/2007GL030215. 957
- Hasselmann, K. (1963), A statistical analysis of the generation 958
of microseisms, *Rev. Geophys.*, *1*, 177–210. 959
- Larose, E., A. Derode, D. Corenec, L. Margerin, and 960
M. Campillo (2005), Passive retrieval of Rayleigh waves in 961
disordered elastic media, *Phys. Rev. E*, *72*, 046607, 962
doi:10.113/PhysRevE.72.046607. 963
- Lin, F., M. H. Ritzwoller, J. Townend, M. Savage, and 964
S. Bannister (2007), Ambient noise Rayleigh wave tomogra- 965
phy of New Zealand, *Geophys. J. Int.*, *170*, 649–666, 966
doi:10.1111/j.1365-246X.2007.03414.x. 967
- Lin, F., M. P. Moschetti, and M. H. Ritzwoller (2008), Surface 968
wave tomography of the western United States from ambient 969
seismic noise: Rayleigh and Love wave phase velocity maps, 970
Geophys. J. Int., in press. 971
- Longuet-Higgins, M. S. (1950), A theory on the origin of 972
microseisms, *Philos. Trans. R. Soc. London*, *243*, 1–35. 973
- Moschetti, M. P., M. H. Ritzwoller, and N. M. Shapiro (2007), Sur- 974
face wave tomography of the western United States from ambient 975
seismic noise: Rayleigh wave group velocity maps, *Geochem.* 976
Geophys. Geosyst., *8*, Q08010, doi:10.1029/2007GC001655. 977
- Nawa, K., N. Suda, Y. Fukao, T. Sato, Y. Aoyama, and 978
K. Shibuya (1998), Incessant excitation of the Earth's free 979
oscillations, *Earth Planets Space*, *50*, 3–8. 980
- Paul, A., M. Campillo, L. Margerin, E. Larose, and A. Derode 981
(2005), Empirical synthesis of time-asymmetrical Green 982
functions from the correlation of coda waves, *J. Geophys.* 983
Res., *110*, B08302, doi:10.1029/2004JB003521. 984
- Rhie, J., and B. Romanowicz (2004), Excitation of Earth's 985
continuous free oscillations by atmosphere-ocean-seafloor, 986
Nature, *431*, 552–556. 987
- Rhie, J., and B. Romanowicz (2006), A study of the relation 988
between ocean storms and the Earth's hum, *Geochem. Geo-* 989
phys. Geosyst., *7*, Q10004, doi:10.1029/2006GC001274. 990



- 991 Sabra, K. G., P. Gerstoft, P. Roux, W. A. Kuperman, and M. C. 1011
992 Fehler (2005), Surface wave tomography from microseism in 1012
993 southern California, *Geophys. Res. Lett.*, *32*, L14311, 1013
994 doi:10.1029/2005GL023155. 276–288.
- 995 Shapiro, N. M., and M. H. Ritzwoller (2002), Monte-Carlo 1014
996 inversion for a global shear velocity model of the crust and 1015
997 upper mantle, *Geophys. J. Int.*, *151*, 88–105. Cause of continuous oscilla-
998 Shapiro, N. M., M. Campillo, L. Stehly, and M. H. Ritzwoller 1016
999 (2005), High resolution surface wave tomography from 1017
1000 ambient seismic noise, *Science*, *307*, 1615–1618. tions of the Earth, *J. Geophys. Res.*, *104*, 28,723–28,739. 1018
- 1001 Shapiro, N. M., M. H. Ritzwoller, and G. D. Bensen (2006), 1019
1002 Source location of the 26 sec microseism from cross correla- 1020
1003 tions of ambient seismic noise, *Geophys. Res. Lett.*, *33*, 1021
1004 L18310, doi:10.1029/2006GL027010. systems and the emergence of the Green's function, *J. Acoust.*
1005 Snieder, R. (2004), Extracting the Green's function from the 1022
1006 correlation of coda waves: A derivation based on stationary 1023
1007 phase, *Phys. Rev. E*, *69*, 046610. *Soc. Am.*, *110*, 3011–3017. 1024
- 1008 Stehly, L., M. Campillo, and N. M. Shapiro (2006), A study of 1025
1009 the seismic noise from its long range correlation properties, 1026
1010 *J. Geophys. Res.*, *111*, B10306, doi:10.1029/2005JB004237. 1027
1011 Tanimoto, T. (2005), The oceanic excitation hypothesis for the 1028
1012 continuous oscillations of the Earth, *Geophys. J. Int.*, *160*, 1029
1013 276–288. maps, *Geophys. J. Int.*, *166*, 732–744. 1030
1014 Tanimoto, T., and J. Um (1999), Cause of continuous oscilla- 1031
1015 tions of the Earth, *J. Geophys. Res.*, *104*, 28,723–28,739. 1032
1016 Weaver, R. L., and O. I. Lobkis (2001), On the emergence of 1033
1017 the Green's function in the correlations of a diffuse field, 1034
1018 *J. Acoust. Soc. Am.*, *110*, 3011–3017. 1035
1019 Weaver, R. L., and O. I. Lobkis (2004), Diffuse fields in open 1036
1020 systems and the emergence of the Green's function, *J. Acoust.*
1021 *Soc. Am.*, *116*, 2731–2734. 1037
1022 Webb, S. C. (1998), Broadband seismology and noise under 1038
1023 the ocean, *Rev. Geophys.*, *36*, 105–142. 1039
1024 Yang, Y., M. H. Ritzwoller, A. L. Levshin, and N. M. Shapiro 1040
1025 (2007), Ambient noise Rayleigh wave tomography across 1041
1026 Europe, *Geophys. J. Int.*, *168*, 259–274. 1042
1027 Yao, H., R. D. van der Hilst, and M. V. De Hoop (2006), 1043
1028 Surface-wave array tomography in SE Tibet from ambient 1044
1029 seismic noise and two-station analysis: I—Phase velocity 1045
1030 maps, *Geophys. J. Int.*, *166*, 732–744. 1046

Article in Progress